

Electronic Supplementary Information

Substituent-Dependent Absorption and Fluorescence Properties of Perylene Bisimide

Radical Anions and Dianions

*Rebecca Renner, Matthias Stolte, Julia Heitmüller, Tobias Brixner, Christoph Lambert, and
Frank Würthner**

* E-mail: wuerthner@uni-wuerzburg.de

Contents

1. General Methods	S2
2. Synthesis	S4
3. Electrochemical Measurements	S7
4. Optical Measurements	S9
5. Theoretical Investigation.....	S17
6. Supporting References	S34

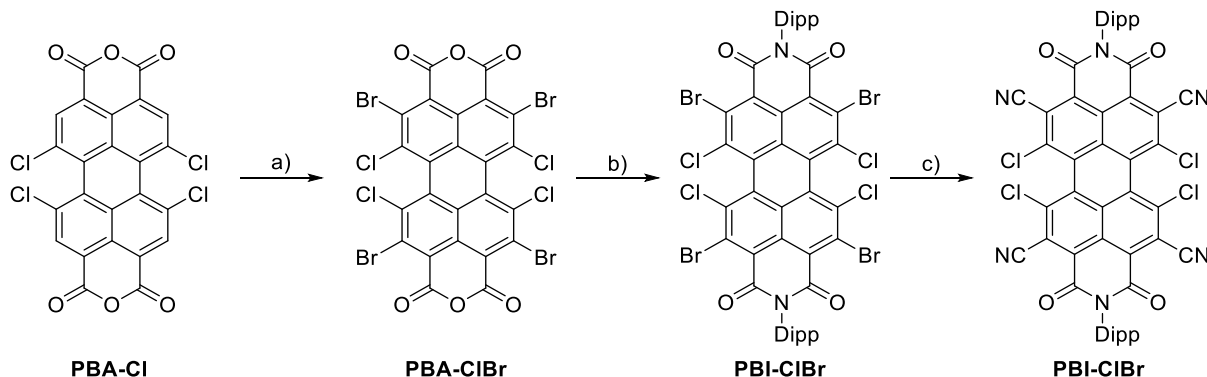
1. General Methods

Unless otherwise stated, all chemicals, reagents and solvents were purchased from commercial suppliers and used after appropriate purification. *N,N'*-Bis(2,6-diisopropylphenyl)-1,6,7,12-tetraphenylperylene-3,4:9,10-bis(dicarboximide) was synthesized according to literature.^[S1] The solvents for the reduction and spectroscopic measurements were of HPLC grade and dried prior to use by an Innovative Technology PureSolv solvent purification system (DCM), by refluxing the solvent over sodium followed by distillation onto sodium (THF) or by refluxing the solvent over molecular sieves (4 Å, 1,2-difluorobenzene). Optical measurements were performed under inert conditions. UV/Vis/NIR absorption spectra were recorded on a Jasco V-770 or V-670 spectrometer. Cyclic and square wave voltammetry measurements were conducted on a standard commercial electrochemical analyzer (EC epsilon, BASi instruments, UK) with a three-electrode single-compartment cell. A Pt disc electrode was used as a working electrode, a platinum wire as a counter electrode and an Ag/AgCl reference electrode using ferrocenium/ferrocene (Fc^+/Fc) as an internal standard for the calibration of the potential. The measurements were carried out under an argon atmosphere in DCM and tetrabutylammonium hexafluorophosphate (TBAHFP) was added as supporting electrolyte, resulting in an available redox window from -2.25 V to +1.75 V (vs. Fc/Fc^+). Spectroelectrochemical absorption measurements were recorded in reflection mode in a three-electrode custom-made cell with a 6 mm diameter Pt-disc working electrode, Pt counter and Ag/AgCl leak free reference electrode implemented in an Agilent Cary 5000 UV/Vis/NIR spectrometer. The optical path was adjusted to 100 µm with a micrometer screw. Potentials were applied with a reference 600 potentiostat (Gamry Instruments). Application of potential steps and recording of absorption spectra was automated by a lab view routine. Fluorescence spectra were measured on a FLS980 fluorescence spectrometer (Edinburgh Instruments) and were corrected against the photomultiplier sensitivity and the lamp intensity. For the fluorescence spectra of the PBI dianions, a custom-built flow cell setup has been built into this spectrometer^[S2] and the

measurements were conducted in front-face geometry (22.5°). The fluorescence lifetimes were determined using picosecond pulsed diode lasers (EPL-series, Edinburgh Instruments) and a PMT-900 fast photomultiplier (Edinburgh Instruments Ltd; Inc) for time correlated single photon counting (TCSCP). The fitting of the data was carried out using the Exp. Tail Fit or the Exp. Reconvolution Fit (for **PBI-CICN**) routine supplied by Edinburgh Instruments Ltd.; Inc. Fluorescence quantum yields of the neutral PBIs were determined using the dilution method ($\text{OD} < 0.05$) and *N,N'*-bis(2,6-diisopropylphenyl)perylene-3,4:9,10-bis(dicarboximide) ($\Phi_f = 1.00$ in CHCl_3) or *N,N'*-bis(2,6-diisopropylphenyl)- 1,6,7,12-tetraphenoxyperylene-3,4:9,10-bis(dicarboximide) (for **PBI-OPh**, $\Phi_f = 0.96$ in CHCl_3)^[S3] as reference. Fluorescence quantum yields of PBI^{2-} were determined relative to the neutral PBI by excitation at 385 nm (**PBI-Cl**), 415 nm (**PBI-H**), 490 nm (**PBI-Ph**) and 398 nm (**PBI-OPh**). Theoretical calculations were performed by the Gaussian software^[S4] using B3LYP/6-31G(d) level theory for structure optimization and B3LYP/def2-SVP (for **PBI-CICN**, **PBI-Cl** and **PBI-H**) or ω B97XD/def2-SVP (for **PBI-Ph** and **PBI-OPh**) level theory for TD-DFT simulation of electron transitions, as these basis sets gave the best results in accordance with the experimental data respectively. Transition densities were calculated using the multiwfn program by T. Lu *et al.*^[S5]

2. Synthesis

PBA-ClBr and **PBI-ClBr** have been synthesized according to previously reported procedures.^[S6] For the synthesis of **PBI-CICN**, a literature known procedure has been modified.^[S7]



Scheme S1 Synthesis of **PBI-CICN** a) DBI, 50% oleum, 100 °C, 18 h, 80%; b) 2,6-diisopropylaniline, propionic acid, reflux, 16 h, 79%; c) CuCN, DMF, 140 °C, 3 h, 9%. DBI = dibromoisocyanuric acid.

A solution of 300 mg (258 µmol) PBI-ClBr and 138 mg (1.55 mmol) copper cyanide in 30 mL of dry DMF was heated to 140 °C for 3 h under argon. After cooling to room temperature, the mixture was poured on water and extracted with dichloromethane. The solvent was removed under reduced pressure and the crude product was purified by column chromatography (dichloromethane) and HPLC (dichloromethane) to give a light red solid.

Yield: 22.2 mg (23.4 µmol, 9%). ¹H NMR (400 MHz, CD₂Cl₂): δ = 7.61 (t, 2H), 7.43 (d, 4H), 2.67 (sept, 4H), 1.21 (d, 12H), 1.20 (d, 12H); ¹³C NMR (100 MHz, CD₂Cl₂): δ = 159.3, 146.0, 140.4, 132.5, 131.0, 129.2, 129.1, 127.4, 125.0, 123.4, 118.7, 113.2, 29.9, 24.21, 24.16; HRMS (ESI, negative mode, acetonitrile/chloroform 1:1): *m/z* calculated for C₅₂H₃₄Cl₄N₆O₄⁻ 946.1401 [M]⁻; found: 946.1430; m.p.>350 °C.

Typical procedure for the chemical reduction

Under an argon atmosphere in a Schlenk flask, the respective PBI (5 μmol), potassium graphite (2.70 mg, 20 μmol , 4 eq) and 18-crown-6 (5.29 mg, 20 μmol , 4 eq) were dissolved in THF and stirred at room temperature for one hour. Afterwards, the solvent was removed *in vacuo* and the residue washed with hexane and toluene. Then the obtained solid was dissolved in 1,2-difluorobenzene and immediately put into a UV/Vis/NIR spectrometer to characterize the obtained species.

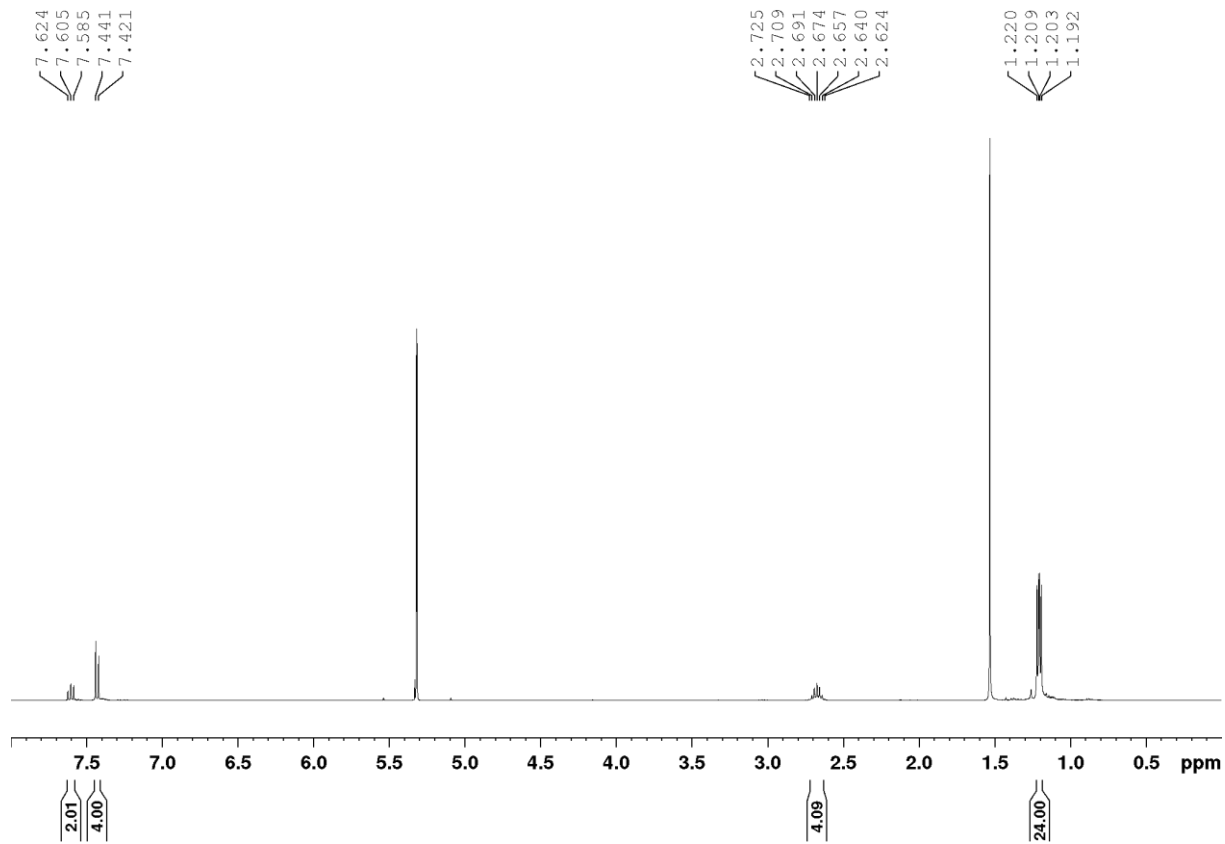


Fig. S1 ^1H NMR (400 MHz) spectrum of **PBI-CICN** in CD_2Cl_2 at room temperature.

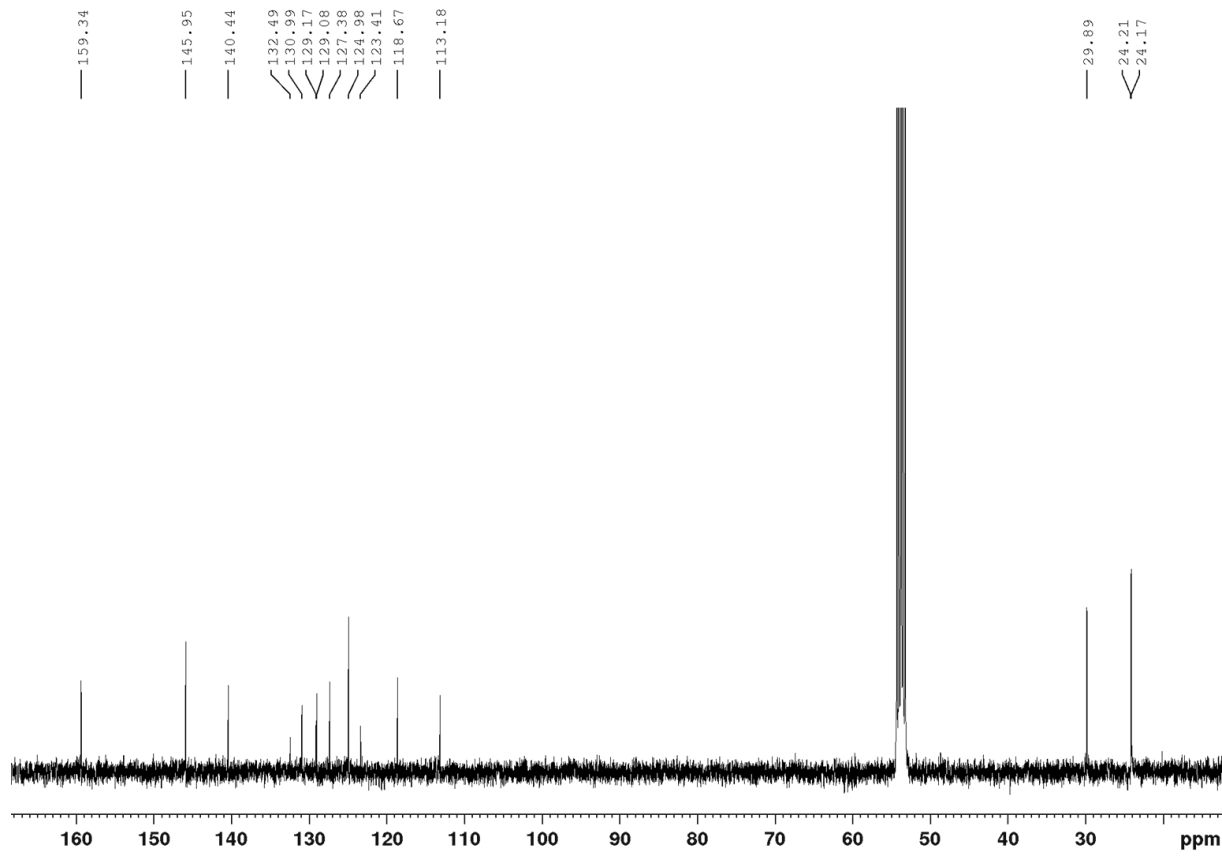


Fig. S2 ^{13}C NMR (100 MHz) spectrum of **PBI-ClCN** in CD_2Cl_2 at room temperature.

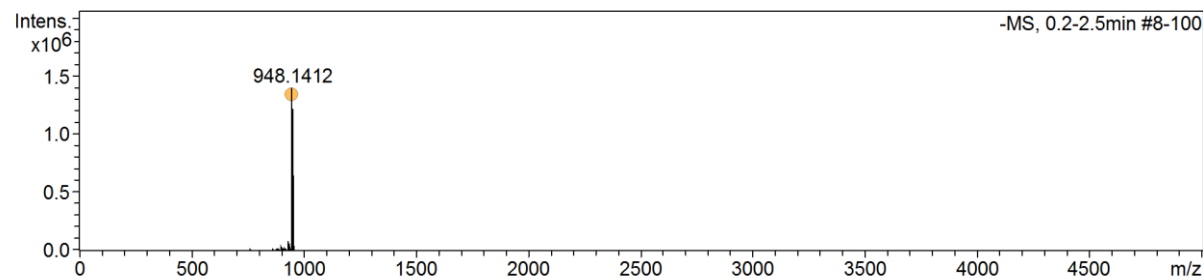


Fig. S3 ESI-MS spectrum of **PBI-ClCN**.

3. Electrochemical Measurements

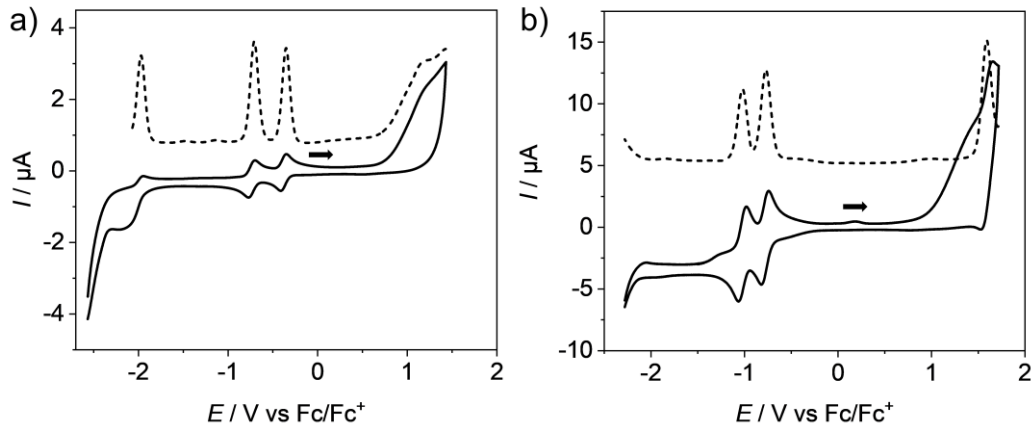


Fig. S4 Cyclic voltammograms (solid lines) and square wave voltammograms (dashed lines) of a) **PBI-CICN** and b) **PBI-Cl**. Measurements were performed using DCM ($c_0 = 2 \cdot 10^{-4}$ M) at room temperature, using TBAHFP (0.1 M) as electrolyte (scan rate 100 mV s⁻¹, the scan direction is indicated by the small arrow, SW amplitude 25 mV, SW frequency 15 Hz).

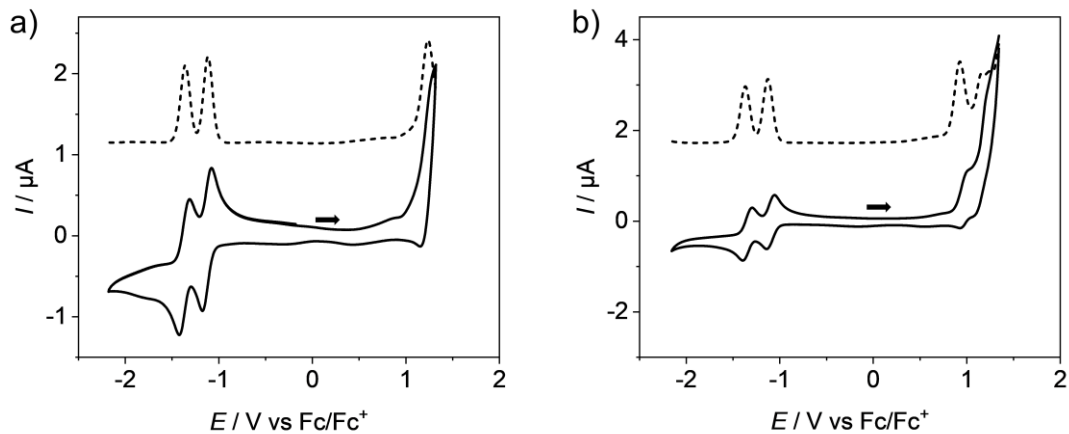


Fig. S5 Cyclic voltammograms (solid lines) and square wave voltammograms (dashed lines) of a) **PBI-H** and b) **PBI-Ph**. Measurements were performed using DCM ($c_0 = 2 \cdot 10^{-4}$ M) at room temperature, using TBAHFP (0.1 M) as electrolyte (scan rate 100 mV s⁻¹, the scan direction is indicated by the small arrow, SW amplitude 25 mV, SW frequency 15 Hz).

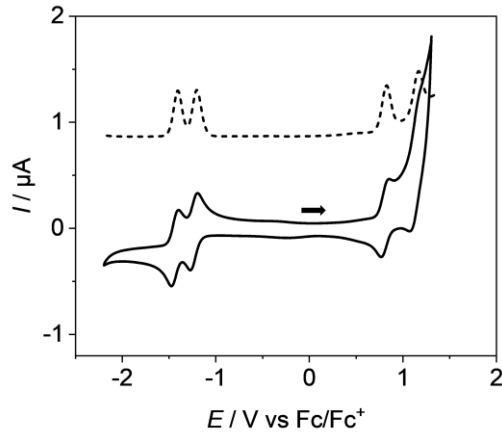


Fig. S6 Cyclic voltammogram (solid line) and square wave voltammogram (dashed line) of **PBI-OPh**. Measurements were performed using DCM ($c_0 = 2 \cdot 10^{-4}$ M) at room temperature, using TBAHFP (0.1 M) as electrolyte (scan rate 100 mV s $^{-1}$, the scan direction is indicated by the small arrow, SW amplitude 25 mV, SW frequency 15 Hz).

Table S1 Electron affinities of the different investigated PBIs as isolated molecule (A_g), as molecular solid (A_c) and in solution (A_{sol}) calculated according to Ref. [S8].

	PBI-CICN	PBI-Cl	PBI-H	PBI-Ph	PBI-OPh
A_g	2.96 eV	2.31 eV	2.07 eV	2.05 eV	1.96 eV
A_c	4.30 eV	3.63 eV	3.38 eV	3.36 eV	3.27 eV
A_{sol}	5.01 eV	4.38 eV	4.15 eV	4.13 eV	4.05 eV

Table S2 Ionization energies of the different investigated PBIs as isolated molecule (I_g), as molecular solid (I_c) and in solution (I_{sol}) calculated according to Ref. [S8].

	PBI-CICN	PBI-Cl	PBI-H	PBI-Ph	PBI-OPh
I_g	-	7.45 eV	6.94 eV	6.43 eV	6.23 eV
I_c	-	6.60 eV	6.17 eV	5.74 eV	5.58 eV
I_{sol}	-	6.74 eV	6.45 eV	6.16 eV	6.05 eV

4. Optical Measurements

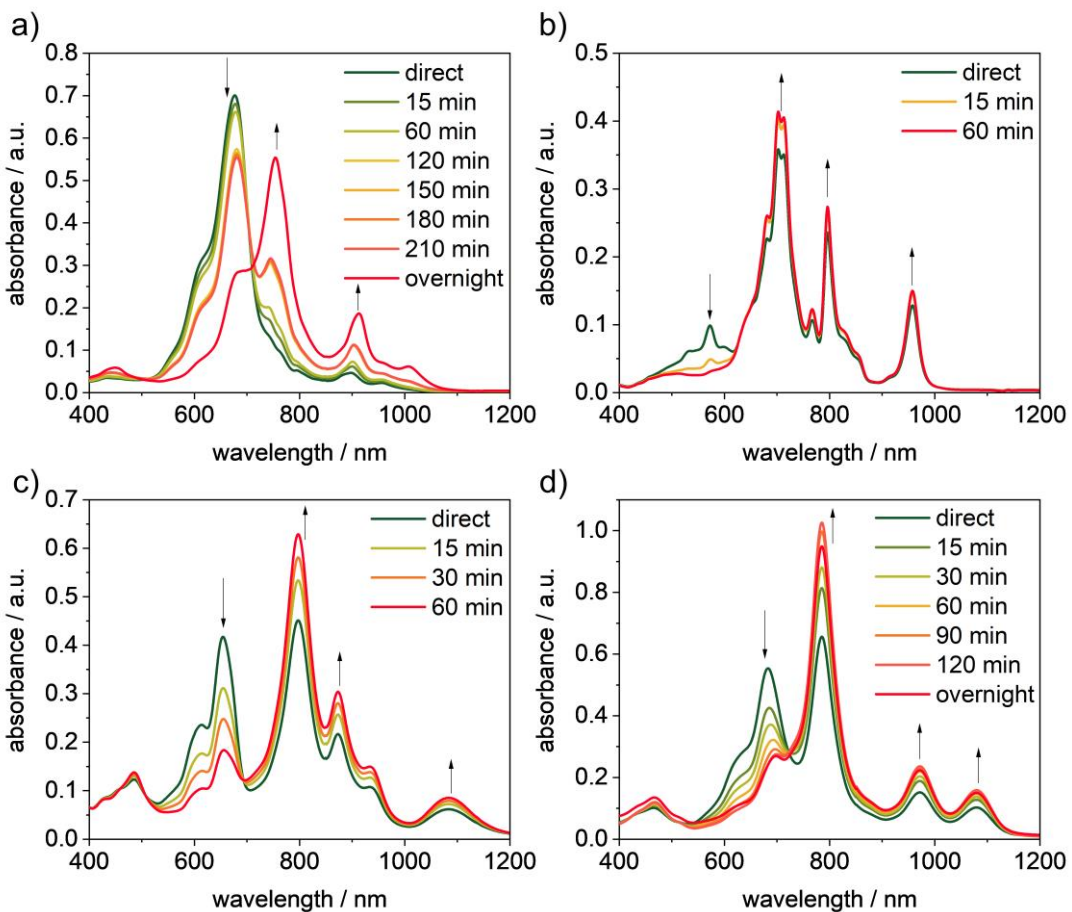


Fig. S7 UV/Vis/NIR absorption spectra of mixed solutions of **PBI²⁻** and **PBI⁻** generated by chemical reduction of a) **PBI-Cl**, b) **PBI-H**, c) **PBI-Ph** and d) **PBI-OPh** with KC_8 measured in 1,2-difluorobenzene at room temperature stored under inert conditions during the measurements.

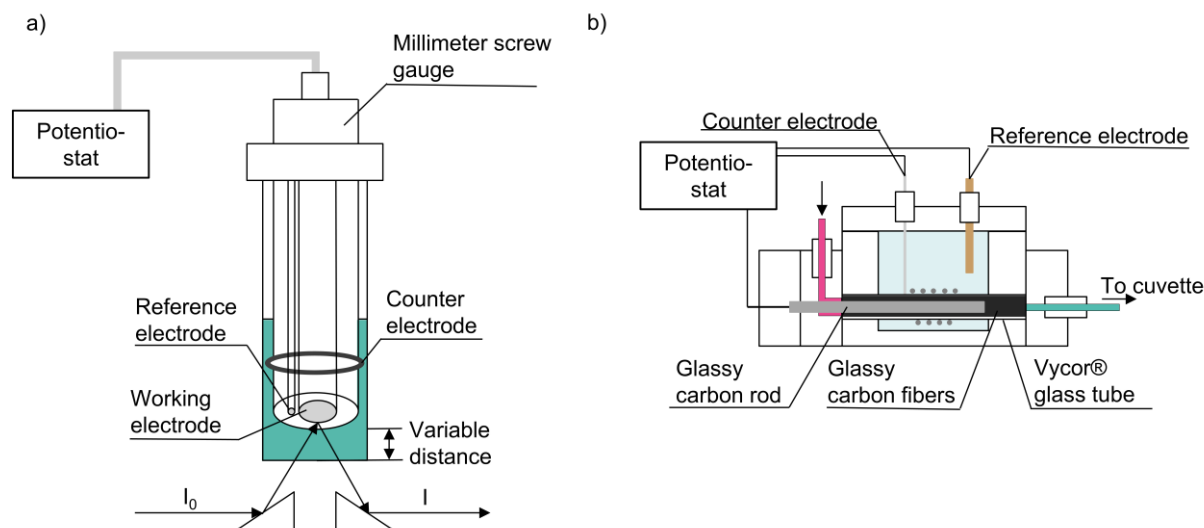


Fig. S8 Schematic illustration of the custom built spectroelectrochemical cells for a) absorption measurements adapted from Borg *et al.*^[S9] and b) fluorescence measurements as described by Heitmüller *et al.* Adapted with permission from Ref. [S2] with permission from Elsevier.

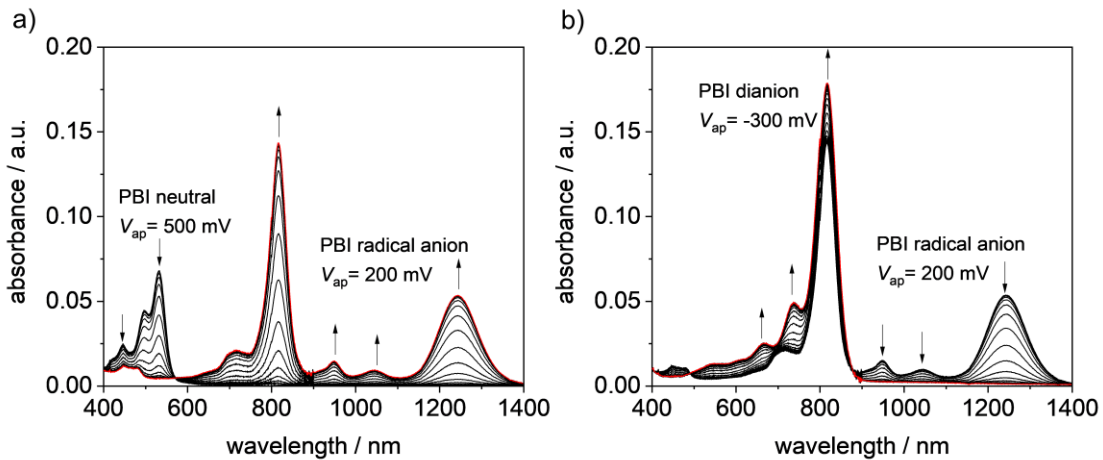


Fig. S9 UV/Vis/NIR absorption changes upon electrochemical reduction of a) **PBI-ClCN** to **PBI-ClCN⁻** (in steps of 20 mV) at potentials from +500 to +200 mV. b) **PBI-ClCN⁻** to **PBI-ClCN²⁻** (in steps of 20 mV) at potentials from +200 to -300 mV ($c_0 = 2 \cdot 10^{-4}$ M, 0.1 M TBAHFP, DCM).

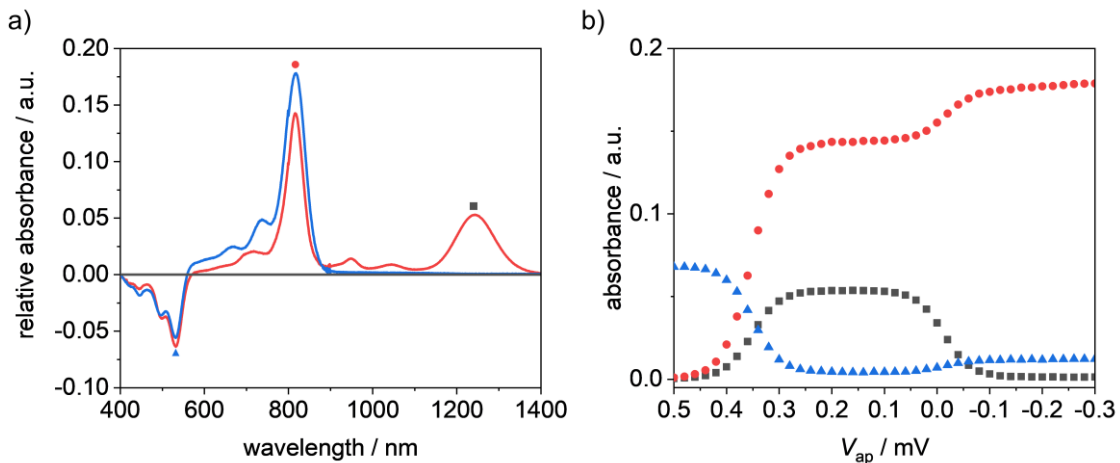


Fig. S10 a) Plots of the relative changes upon reduction of **PBI-ClCN** compared to the neutral state; b) Plots of the absorbance in dependence of the applied voltage V_{ap} at 1243 nm (grey squares), 817 nm (red circle) and 531 nm (blue triangle).

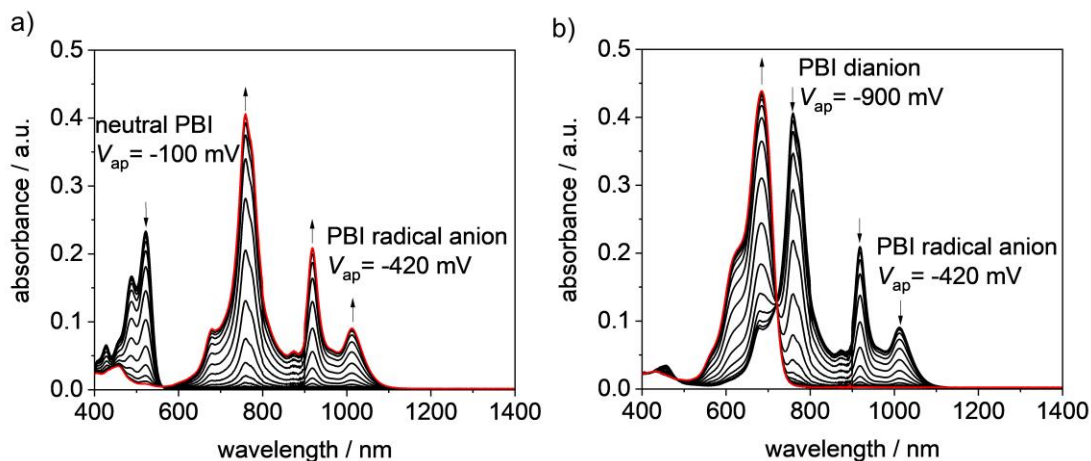


Fig. S11 UV/Vis/NIR absorption changes upon electrochemical reduction of a) **PBI-Cl** to **PBI-Cl⁻** (in steps of 20 mV) at potentials from -100 to -420 mV; b) **PBI-Cl⁻** to **PBI-Cl²⁻** (in steps of 20 mV) at potentials from -420 to -900 mV ($c_0 = 4 \cdot 10^{-4}$ M, 0.1 M TBAHFP, DCM).

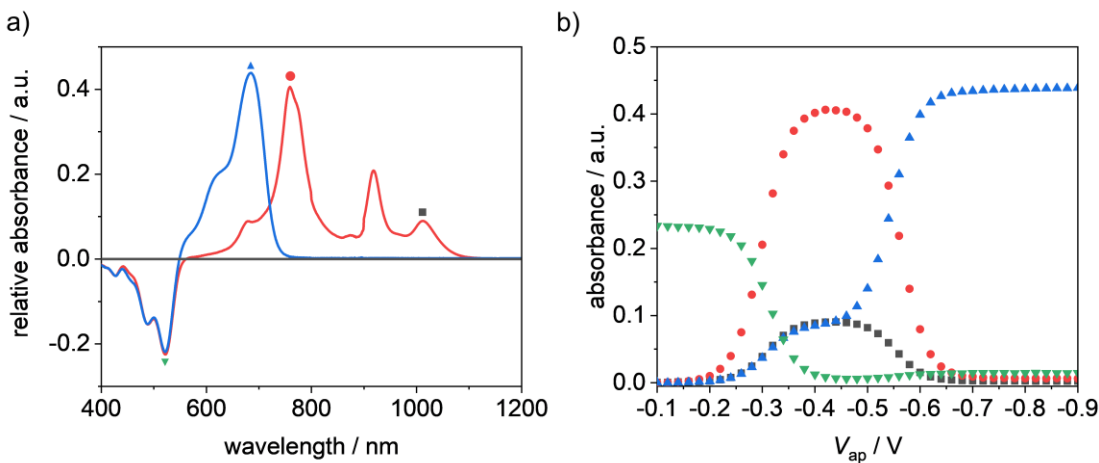


Fig. S12 a) Plots of the relative changes upon reduction of **PBI-Cl** compared to the neutral state; b) Plots of the absorbance in dependance of the applied voltage V_{ap} at 1011 nm (grey squares), 759 nm (red circle), 684 nm (blue triangle) and 522 nm (green inverse triangle).

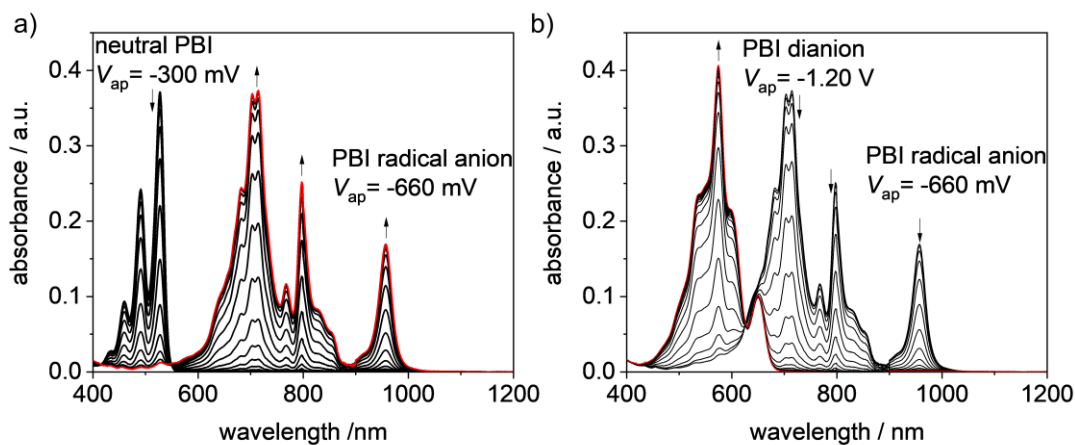


Fig. S13 UV/Vis/NIR absorption changes upon electrochemical reduction of a) **PBI-H** to **PBI-H^{•-}** (in steps of 20 mV) at potentials from -300 to -660 mV; b) **PBI-H^{•-}** to **PBI-H^{2•-}** (in steps of 20 mV) at potentials from -660 mV to -1.20 V ($c_0 = 4 \cdot 10^{-4}$ M, 0.1 M TBAHFP, DCM).

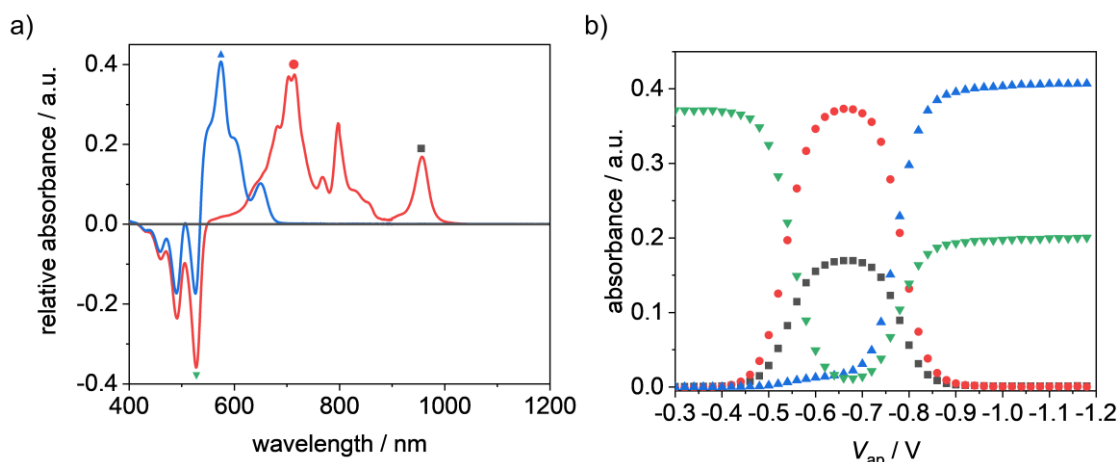


Fig. S14 a) Plots of the relative changes upon reduction of **PBI-H** compared to the neutral state; b) Plots of the absorbance in dependence of the applied voltage V_{ap} at 957 nm (grey squares), 715 nm (red circle), 574 nm (blue triangle) and 527 nm (green inverse triangle).

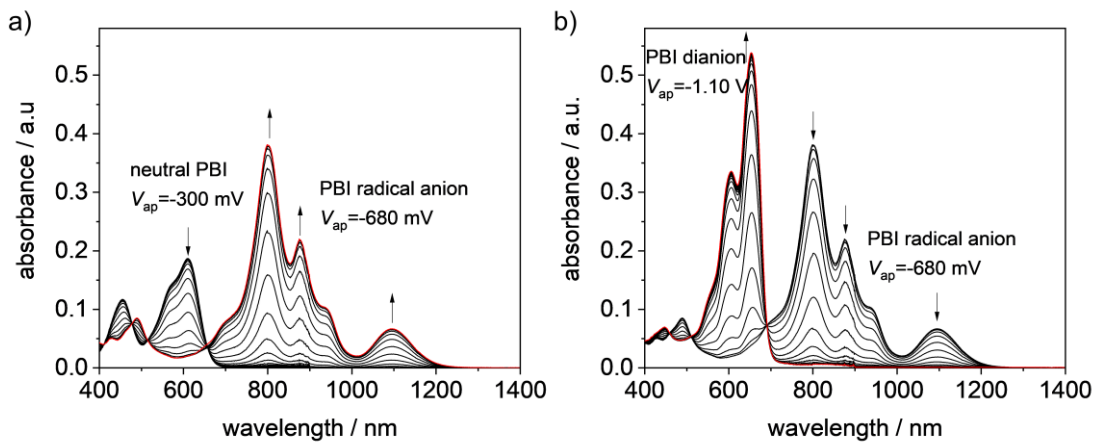


Fig. S15 UV/Vis/NIR absorption changes upon electrochemical reduction of a) **PBI-Ph** to **PBI-Ph^{•-}** (in steps of 20 mV) at potentials from -300 to -680 mV. b) **PBI-Ph^{•-}** to **PBI-Ph²⁻** (in steps of 20 mV) at potentials from -680 to -1.10 V ($c_0 = 8 \cdot 10^{-4}$ M, 0.1 M TBAHFP, DCM).

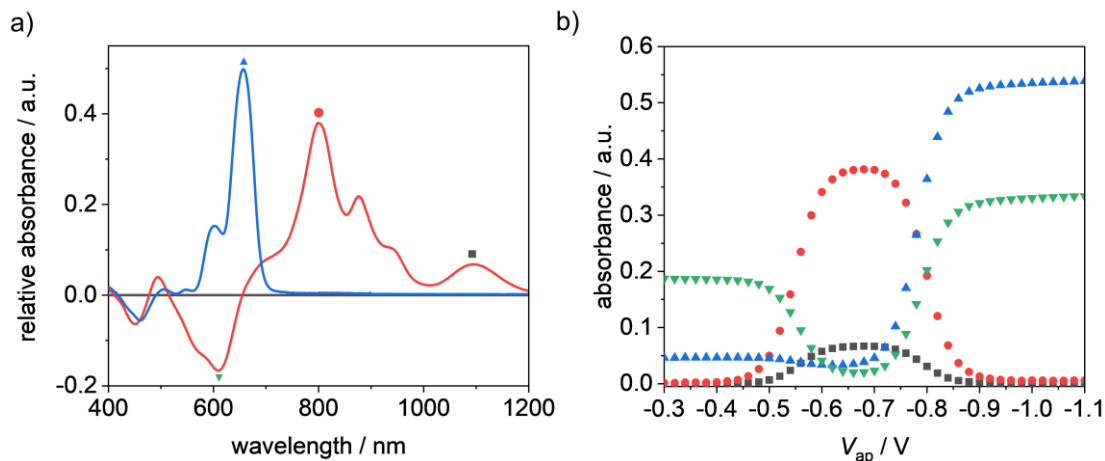


Fig. S16 a) Plots of the relative changes upon reduction of **PBI-Ph** compared to the neutral state; b) Plots of the absorbance in dependence of the applied voltage V_{ap} at 1097 nm (grey squares), 799 nm (red circle), 653 nm (blue triangle) and 609 nm (green inverse triangle).

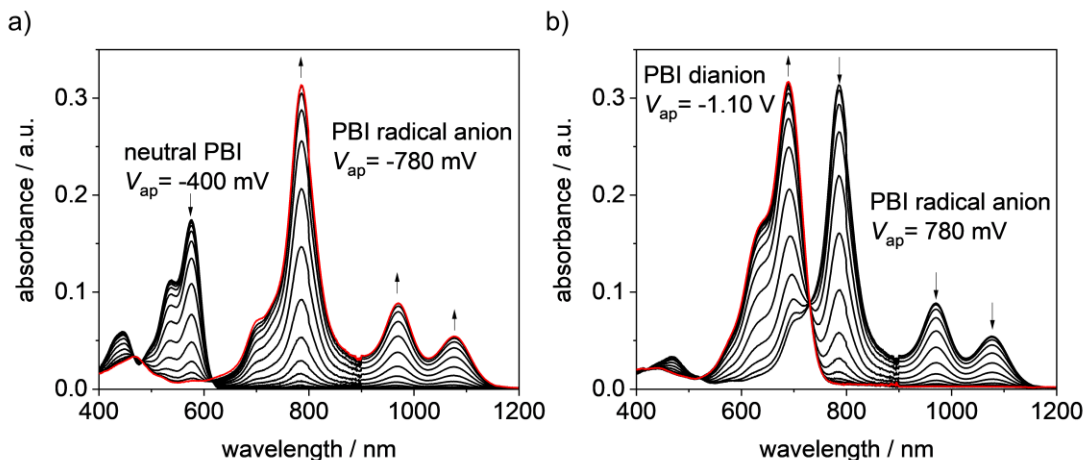


Fig. S17 UV/Vis/NIR absorption changes upon electrochemical reduction of c) **PBI-OPh** to **PBI-OPh^{•-}** (in steps of 20 mV) at potentials from -400 to -780 mV; d) **PBI-OPh^{•-}** to **PBI-OPh²⁻** (in steps of 20 mV) at potentials from -780 mV to -1.10 V ($c_0 = 3.6 \cdot 10^{-4}$ M, 0.1 M TBAHFP, DCM).

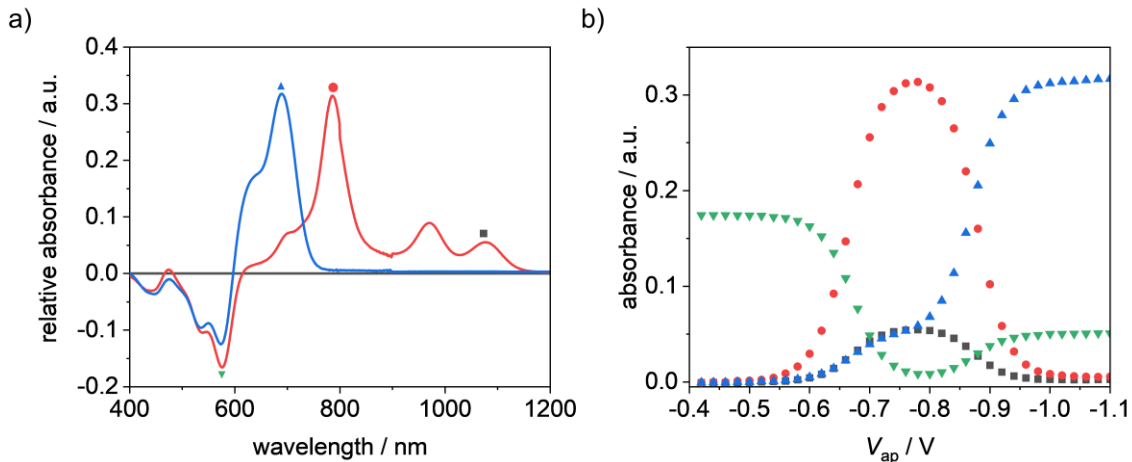


Fig. S18 a) Plots of the relative changes upon reduction of **PBI-OPh** compared to the neutral state; b) Plots of the absorbance in dependance of the applied voltage V_{ap} at 1076 nm (grey squares), 785 nm (red circle), 689 nm (blue triangle) and 576 nm (green inverse triangle).

Table S3 Summary of the absorption properties of the investigated PBIs and their electrochemical reduced species measured in DCM (0.1 M TBAHFP) at room temperature.

	λ_{abs} [nm]			ε_{max} [$M^{-1} cm^{-1}$]		
	PBI	PBI ⁻	PBI ²⁻	PBI	PBI ⁻	PBI ²⁻
PBI-CICN	531*	1243	817*	33900*	26100	87200*
	496	1043	737	22100	4800	24200
	446	947	669	12200	7400	12300
		817*			70300*	
		714			10700	
PBI-Cl	522*	1011	684*	58200*	22100	109100*
	489	918		41600	51800	
	428	759*		16300	101100*	
		679			22000	
PBI-H	527*	957	649	93700*	42800	25600
	491	797	574*	61300	63500	102600*
	459	768		23600	29500	
		715*			94100*	
		703			93000	
		682			61700	
PBI-Ph	609*	1097	653*	23400*	8300	67300*
	454	877	606	14600	27300	4200
		799*	447		47600*	8800
		489			10600	
PBI-OPh	576*	1076	689*	49600*	15100	88700*
	539	971		31900	24800	
	443	785*		16700	88700*	

*main absorption peak.

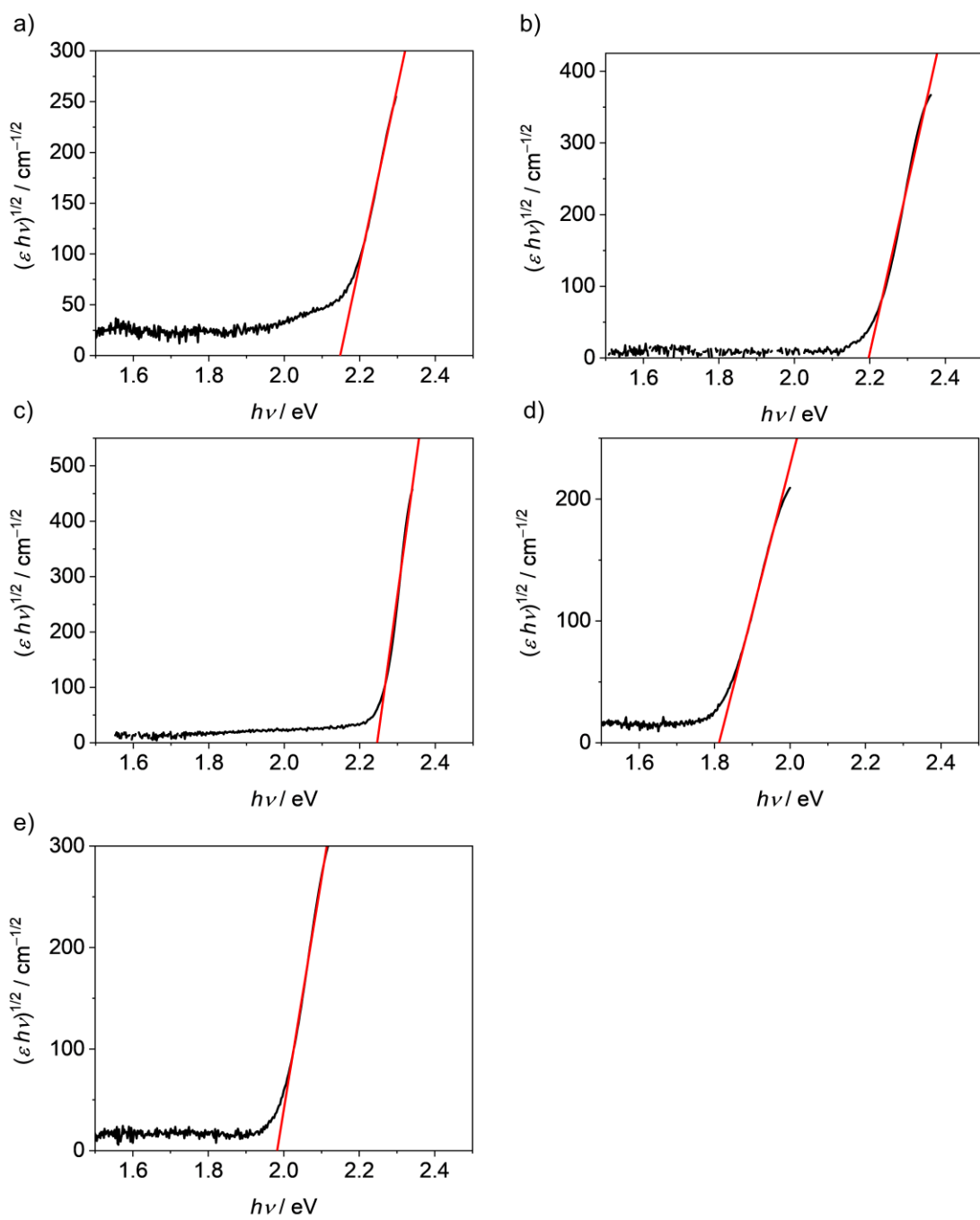


Fig. S19 Tauc plots (black) including the linear fit (red) of a) **PBI-CICN**, b) **PBI-Cl**, c) **PBI-H**, d) **PBI-Ph** and e) **PBI-OPh**. The absorption band used to obtain the Tauc plots always corresponds to the S₀-S₁ transition of the neutral PBI.

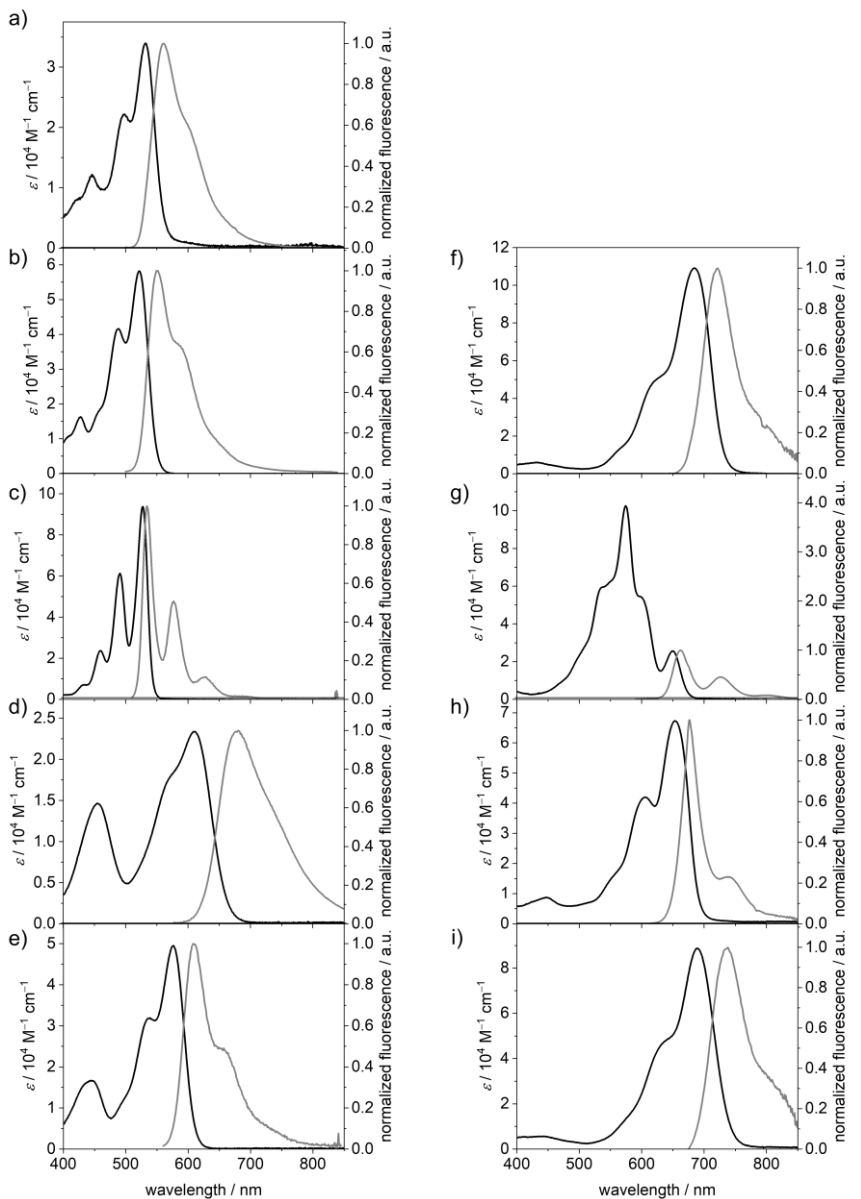


Fig. S20 UV/Vis/NIR absorption and fluorescence emission spectra of the neutral (a-e) and dianionic (f-i) PBI species of a) **PBI-CICN**; b), f) **PBI-Cl**; c), g) **PBI-H**; d), h) **PBI-Ph**; and e), i) **PBI-OPh** measured in DCM ($c_0 = 4 \cdot 10^{-4}$ M for absorption, $c_0 = 1 \cdot 10^{-5}$ M for fluorescence of PBI and $c_0 = 1 \cdot 10^{-4}$ M for fluorescence of PBI^{2-}) at room temperature using TBAHFP (0.1 M) as electrolyte.

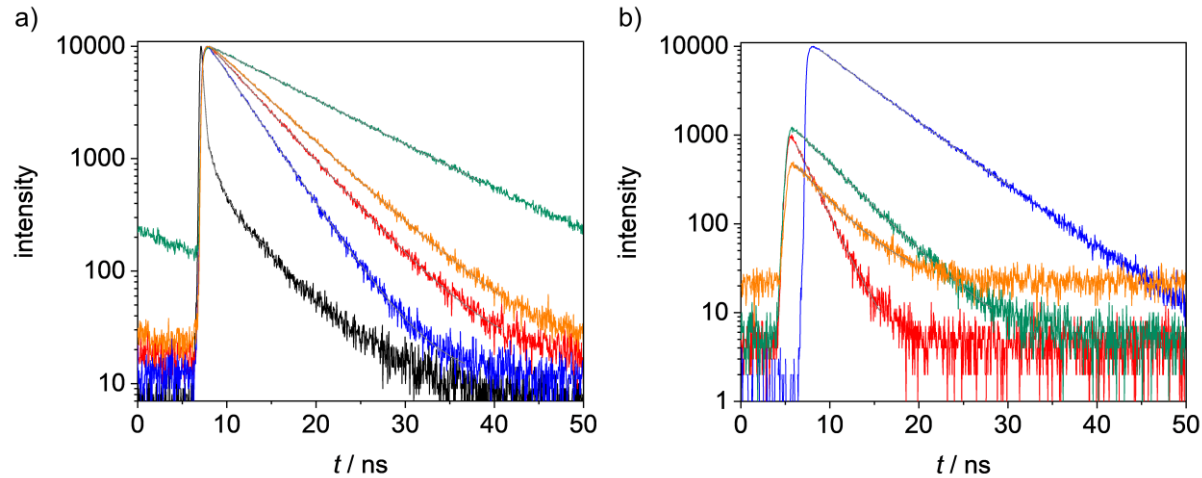


Fig. S21 Fluorescence decay in dichloromethane at 293 K for **PBI-ClCN** (black), **PBI-Cl** (red), **PBI-H** (blue), **PBI-Ph** (green) and **PBI-OPh** (orange) in their a) neutral as well as b) dianionic state ($c_0 = 1 \cdot 10^{-5}$ M for lifetime of PBI and $c_0 = 1 \cdot 10^{-4}$ M for lifetime of PBI^{2-}).

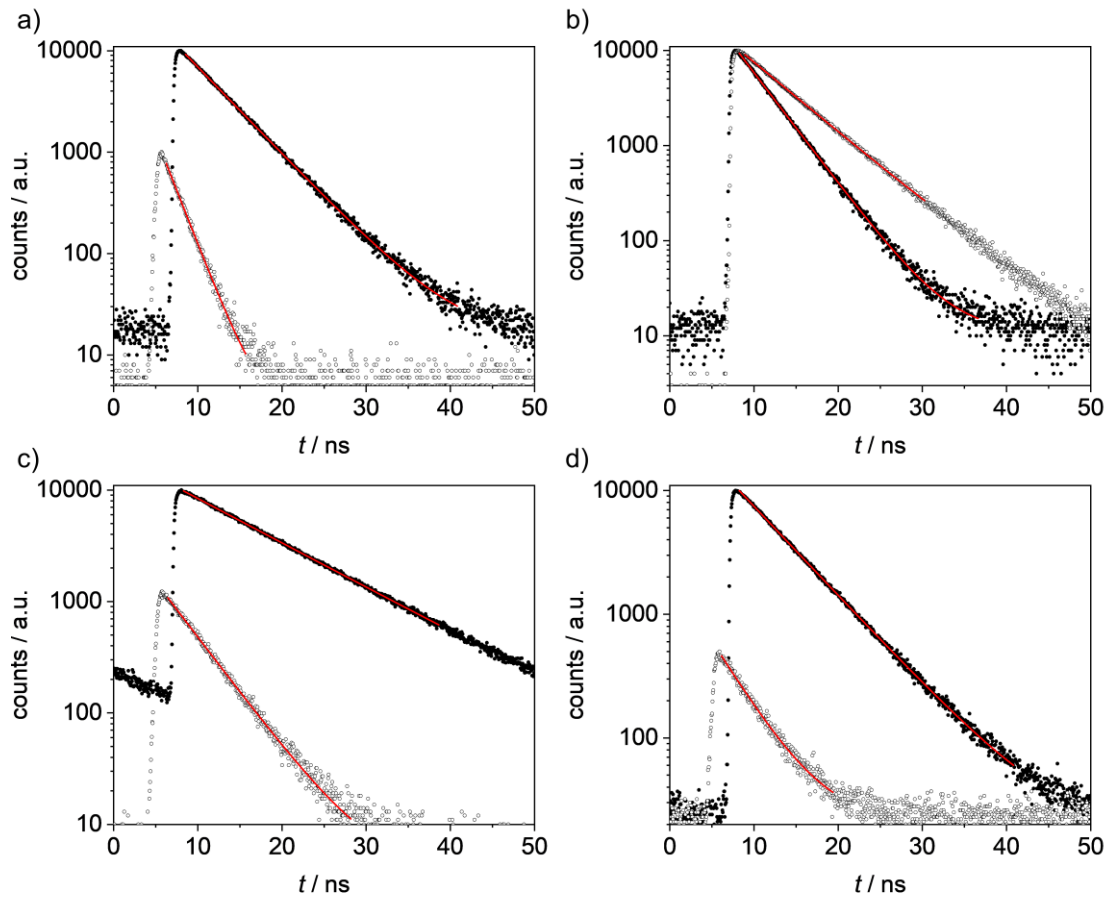


Fig. S22 Fluorescence decay of the neutral (solid circles) and dianionic (open circles) a) **PBI-Cl**, b) **PBI-H**, c) **PBI-Ph** and d) **PBI-OPh** in dichloromethane at 293 K ($c_0 = 1 \cdot 10^{-5}$ M for lifetime of PBI and $c_0 = 1 \cdot 10^{-4}$ M for lifetime of PBI^{2-}).

5. Theoretical Investigation

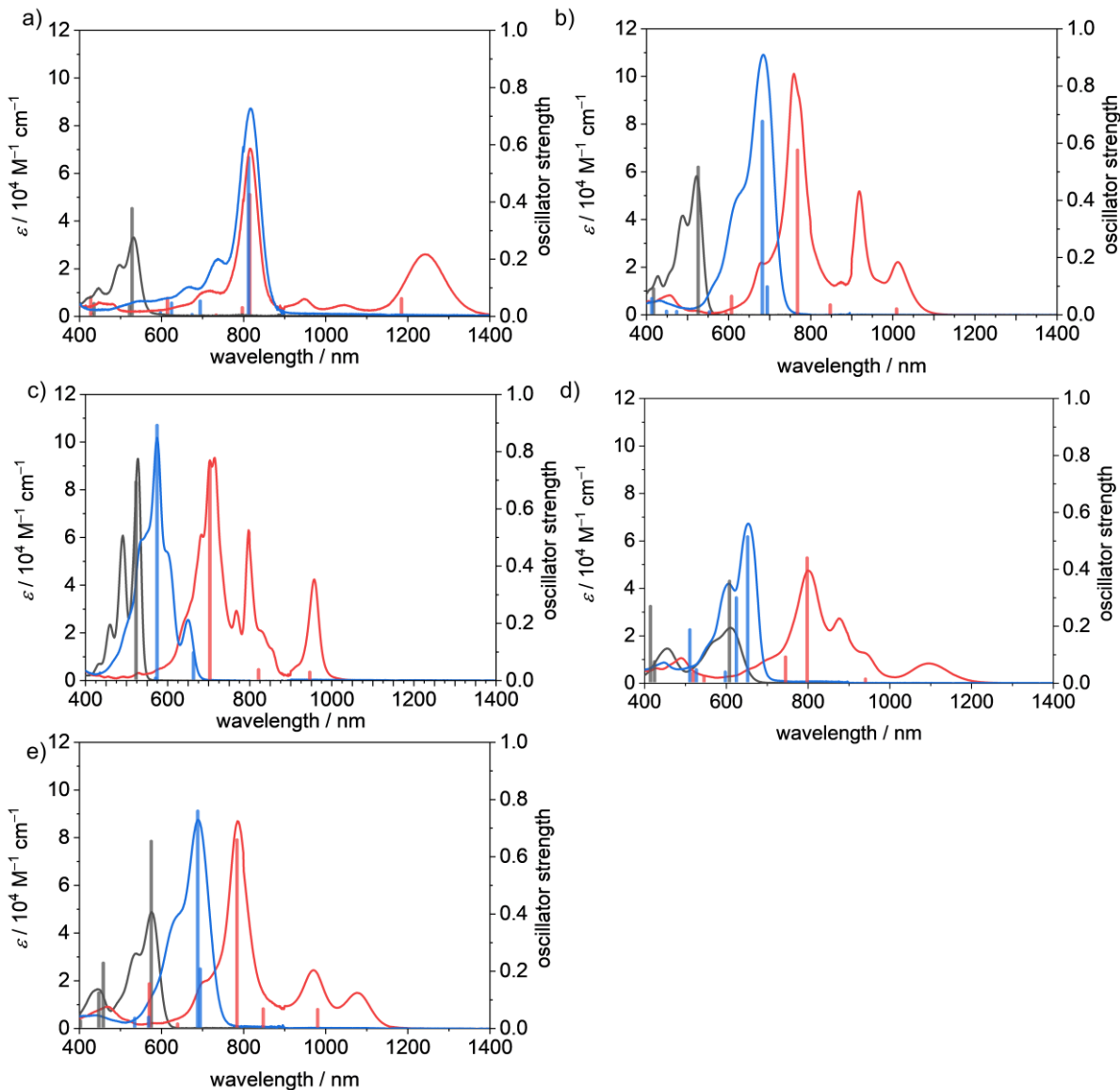


Fig. S23 UV/Vis/NIR absorption spectra of **PBI** (dark grey) and the electrochemically generated **PBI**⁻ (red) and **PBI**²⁻ (blue) of a) **PBI-CiCN**, b) **PBI-Cl**, c) **PBI-H**, d) **PBI-Ph** and e) **PBI-OPh** measured in DCM ($c_0 = 4 \cdot 10^{-4} \text{ M}$) at room temperature using TBAHFP (0.1 M) as electrolyte, as well as the calculated transitions thereof (lighter color) using TD-DFT (a) – c) B3LYP/def-SVP and d)-e) ω B97XD/def2-SVP).

The calculated transitions in Fig. S23 have been shifted, so that the transition with the highest oscillator strength corresponds in energy to the wavelength of the absorption maximum.

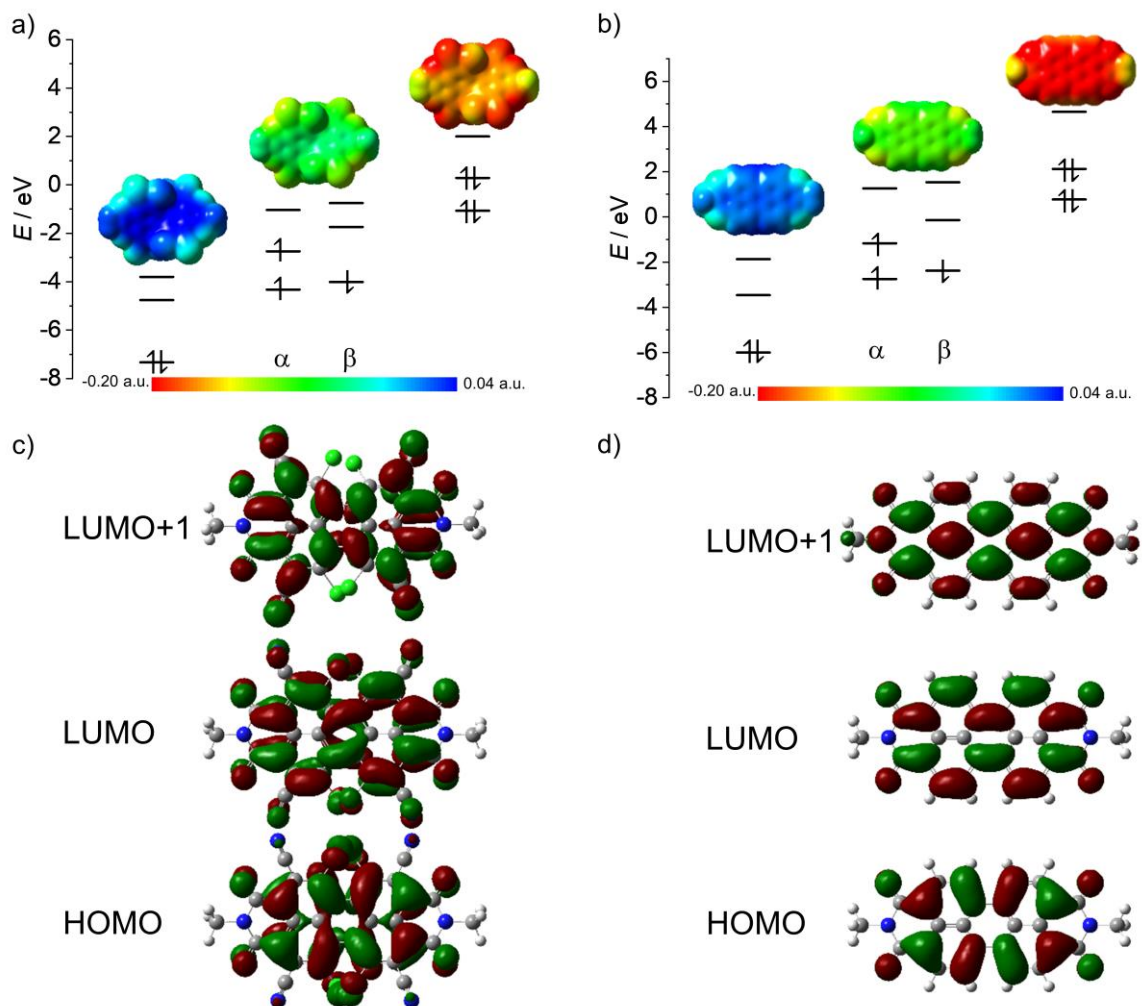


Fig. S24 HOMO, LUMO and LUMO+1 levels as obtained from DFT calculations of a) PBI-CICN (left), the corresponding α - and β -spin MO levels of PBI-CICN^{•-} (middle) and HOMO–1, HOMO and LUMO levels of PBI-CICN²⁻ (right), as well as the electrostatic potential maps of the respective derivative (top, isovalue 0.020 a.u.) and b) PBI-H as well as the respective reduced states. HOMO, LUMO and LUMO+1 (bottom to top) of c) PBI-CICN and d) PBI-H. The corresponding orbitals of PBI-CICN^{•-} and PBI-CICN²⁻ and PBI-H^{•-} and PBI-H²⁻ respectively are visually indistinguishable. Orbitals and electrostatic potential maps were calculated using DFT (B3LYP/6-31g(d)).

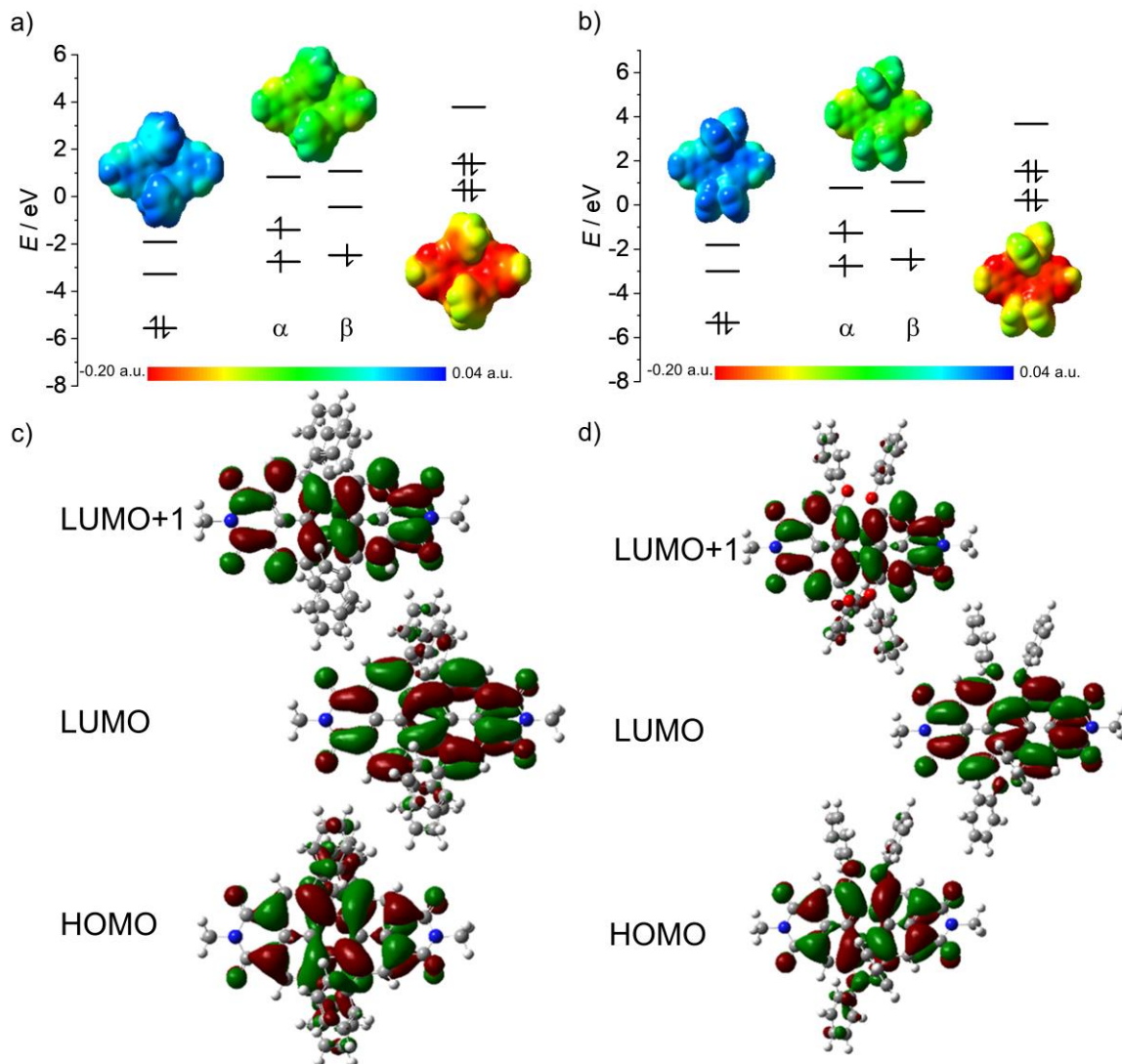


Fig. S25 HOMO, LUMO and LUMO+1 levels as obtained from DFT calculations of a) **PBI-Ph** (left), the corresponding α - and β -spin MO levels of **PBI-Ph $^{\bullet-}$** (middle) and HOMO–1, HOMO and LUMO levels of **PBI-Ph $^{2-}$** (right), as well as the electrostatic potential maps of the respective derivative (top, isovalue 0.020 a.u.) and b) **PBI-OPh** as well as the respective reduced states. HOMO, LUMO and LUMO+1 (bottom to top) of c) **PBI-Ph** and d) **PBI-OPh**. The corresponding orbitals of **PBI-Ph $^{\bullet-}$** and **PBI-Ph $^{2-}$** and **PBI-OPh $^{\bullet-}$** and **PBI-OPh $^{2-}$** respectively are visually indistinguishable. Orbitals and electrostatic potential maps were calculated using DFT (B3LYP/6-31g(d)).

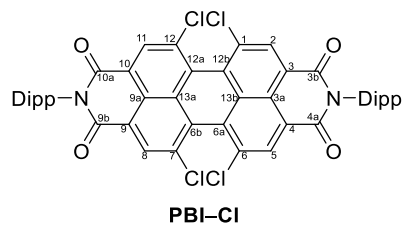


Fig. S26 Chemical structures and atom numbering of **PBI-Cl**.

Table S4 Comparison of the calculated bond distances and torsion angles of **PBI-Cl**, **PBI-Cl⁻** and **PBI-Cl²⁻**. The numbering of carbon atoms is according to Fig. S18.

	PBI-Cl	PBI-Cl⁻	PBI-Cl²⁻
C-C (C6a-C6b, C12a-C12b)	146.8 pm	144.8 pm	143.1 – 143.2 pm
C-C (C1-C2, C5-C6, C7-C8, C11-C12)	140.6 pm	138.6 pm	136.9 – 137.0 pm
C-C (C2-C3, C4-C5, C8-C9, C10-C11)	138.0 pm	139.6 – 139.7 pm	141.3 – 141.4 pm
C-C (C3-C3a, C4-C3a, C9-C9a, C10-C9a)	141.3 pm	141.4 – 141.5 pm	141.6 – 141.7 pm
C-C (C3a-C13b, C9a-C13a)	142.0 pm	142.9 pm	143.9 pm
C-C (C13b-C12b, C13b-C6a, C13a-C6b, C13a-C12a)	143.5 pm	143.6 pm	143.8 pm
C-C (C1-C12b, C6-C6a, C7-C6b, C12-C12a)	140.4 pm	142.2 pm	143.8 – 143.9 pm
C-C (C3-C3b, C4-C4a, C9-C9b, C10-C10a)	148.5 pm – 148.6 pm	146.5 – 146.6 pm	144.7 pm
Torsion angle	35.4°	33.4°/33.5°	31.2°/31.4°

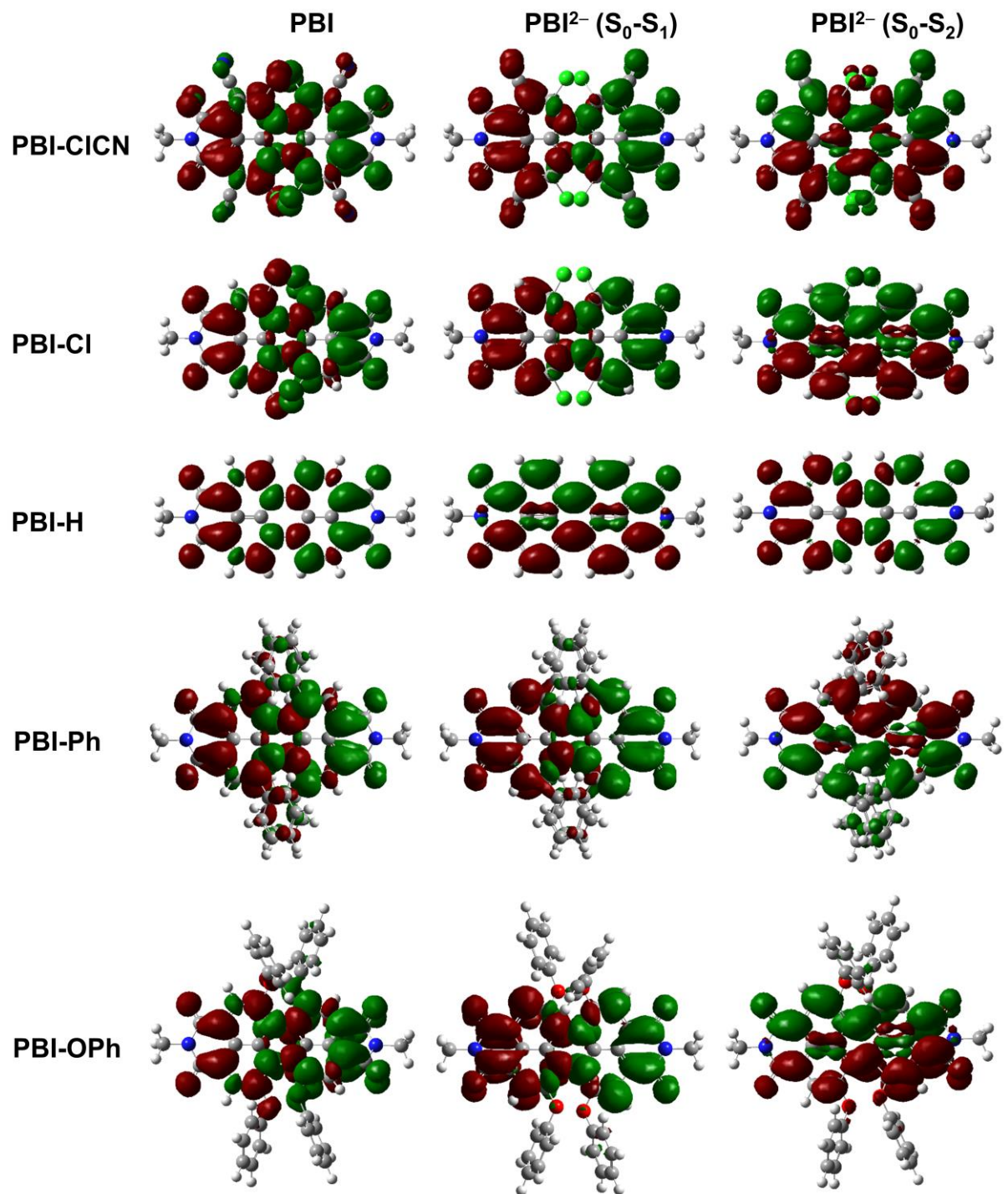


Fig. S27 Transition densities (isovalue = 0.0004 a.u.) of the neutral S_0-S_1 (left) and dianionic S_0-S_1 (middle) as well as dianionic S_0-S_2 (right) transitions of **PBI-CICN**, **PBI-Cl**, **PBI-H**, **PBI-Ph** and **PBI-OPh**.

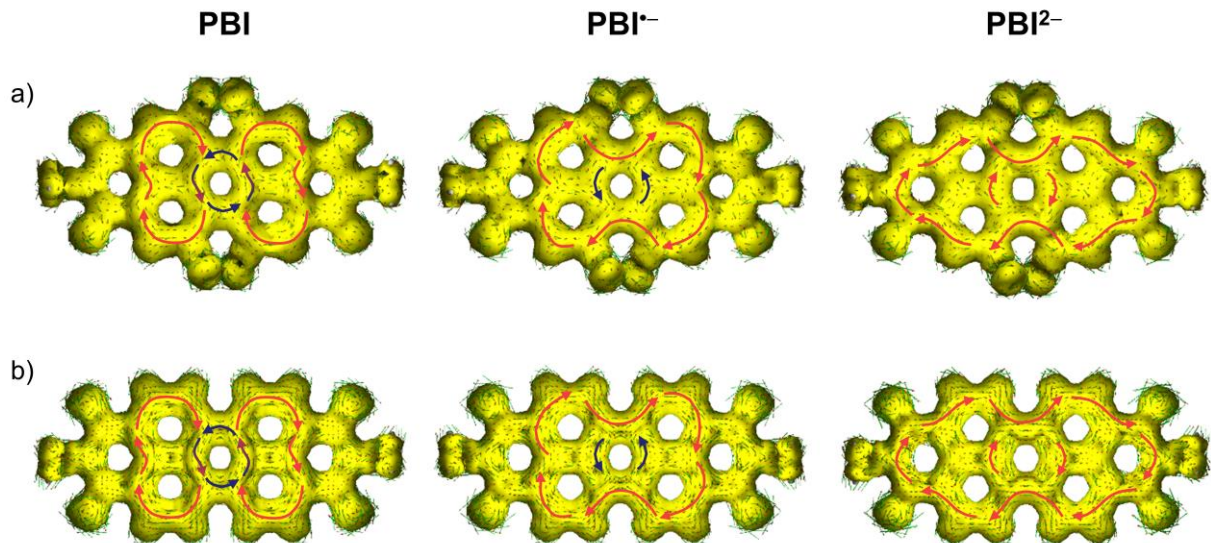


Fig. S28 Calculated AICD isosurface plots of PBI, PBI⁻ and PBI²⁻ of a) **PBI-Cl** and b) **PBI-H**. Clockwise ring current is depicted with red arrows and counter clockwise ring current with blue arrows (isosurface value 0.025).

Table S5 Calculated UV/Vis/NIR transitions for **PBI-CICN**.

Transitions	% character	λ_{cal} [nm]	Oscillator strength f
162 → 165	6.53	571.03	0.3743
164 → 165	93.5		
162 → 165	88.5	564.01	0.0302
163 → 166	4.49		
164 → 165	7.02		
157 → 165	9.01	464.71	0.410
159 → 165	28.7		
161 → 165	62.3		
156 → 165	34.3	460.32	0.0028
158 → 165	20.3		
160 → 165	45.4		
155 → 165	2.52	455.02	0.0641
156 → 165	2.40		
157 → 165	32.6		
159 → 165	27.0		
161 → 165	35.5		
156 → 165	8.81	438.60	0.0187
158 → 165	39.9		
160 → 165	49.0		
164 → 169	2.26		
154 → 165	3.32	425.93	0.0082
156 → 165	53.5		
158 → 165	37.0		
160 → 165	6.18		
155 → 165	15.0	419.07	0.0158
157 → 165	11.5		
159 → 165	9.96		
164 → 166	52.4		
155 → 165	15.2	416.80	0.0492
157 → 165	30.5		
159 → 165	35.4		
164 → 166	18.9		

Table S6 Calculated UV/Vis/NIR transitions for **PBI-CICN^{•-}**.

Transitions	% character	λ_{cal} [nm]	Oscillator strength f
165A → 166A 164B → 165B	75.9 24.1	1036.86	0.0585
165A → 166A 164B → 165B 165A ← 166A	24.3 74.5 1.2	665.96	0.4235
165A → 167A 161B → 165B	98.4 1.58	647.56	0.0267
165A → 168A	100	584.36	0.0011
160A → 166A 164A → 168A 159B → 165B 160B → 166B 161B → 165B	2.91 1.60 1.13 1.62 92.7	465.21	0.0597
161A → 166A 158B → 165B 160B → 165B 161B → 166B	4.14 2.39 90.5 3.01	448.09	0.0090

Table S7 Calculated UV/Vis/NIR transitions for **PBI-CICN²⁻**.

Transitions	% character	λ_{cal} [nm]	Oscillator strength f
165 → 166 165 ← 166	95.1 4.92	719.15	0.5538
165 → 167 165 → 169	83.6 16.4	601.17	0.0499
165 → 168	100	581.34	0.0029
165 → 167 165 → 169	15.5 84.5	531.39	0.0429
164 → 167 164 → 169 165 → 171	2.21 4.32 93.5	342.52	0.0047

Table S8 Calculated UV/Vis/NIR transitions for **PBI-Cl**.

Transitions	% character	λ_{cal} [nm]	Oscillator strength f
140 → 141	100	526.58	0.5139
139 → 141	97.5	418.46	0.0874
140 → 145	2.48		
136 → 141	100	393.88	0.0058
131 → 142	2.15	372.17	0.0268
132 → 141	35.6		
133 → 141	12.7		
135 → 141	49.5		
130 → 141	3.66	370.97	0.0073
131 → 141	32.0		
134 → 141	64.4		
132 → 141	5.34	631.66	0.0038
133 → 141	27.9		
135 → 141	4.45		
140 → 142	62.3		
130 → 141	18.3	358.91	0.0040
131 → 141	58.9		
134 → 141	20.1		
140 → 143	2.69		
132 → 141	47.8	355.69	0.0536
133 → 141	4.46		
135 → 141	47.8		

Table S9 Calculated UV/Vis/NIR transitions for **PBI-Cl⁻**.

Transitions	% character	λ_{cal} [nm]	Oscillator strength f
141A → 142A	61.4	830.49	0.0172
140B → 141B	38.6		
141A → 143A	98.6	667.64	0.0311
139B → 141B	1.38		
141A → 142A	38.9	587.89	0.5735
140B → 141B	61.1		
141A → 144A	2.17	427.16	0.0617
139B → 141B	97.8		
136B → 142B	2.68	414.57	0.0015
137B → 141B	93.1		
138B → 142B	3.09		
139B → 141B	1.15		

Table S10 Calculated UV/Vis/NIR transitions for **PBI-Cl²⁻**.

Transitions	% character	λ_{cal} [nm]	Oscillator strength f
141 → 143	100	583.22	0.0947
141 → 142	96.98	571.34	0.6747
141 ← 142	3.02		
141 → 144	100	441.88	0.0074
140 → 143	3.40	362.02	0.0082
141 → 145	4.81		
141 → 146	91.8		
140 → 143	97.4	337.46	0.0090
141 → 146	2.64		
141 → 149	41.3	300.87	0.0534
141 → 150	58.7		

Table S11 Calculated UV/Vis/NIR transitions for **PBI-H**.

Transitions	% character	λ_{cal} [nm]	Oscillator strength f
108 → 109	97.4	524.36	0.6922
108 ← 109	2.59		
102 → 109	23.8	380.11	0.0049
104 → 109	76.2		
102 → 109	74.9	365.08	0.0015
104 → 109	25.1		

Table S12 Calculated UV/Vis/NIR transitions for **PBI-H^{•-}**.

Transitions	% character	λ_{cal} [nm]	Oscillator strength f
109A → 111A 108B → 109B	27.1 72.9	773.90	0.0253
109A → 110A	100	648.62	0.0342
103A → 110A 109A → 111A 108B → 109B	1.17 72.8 26.1	530.10	0.7603

Table S13 Calculated UV/Vis/NIR transitions for **PBI-H²⁻**.

Transitions	% character	λ_{cal} [nm]	Oscillator strength f
109 → 110	100	570.61	0.0938
109 → 111 109 ← 111	97.9 2.07	482.09	0.8905
109 → 112	100	487.44	0.0044

Table S14 Calculated UV/Vis/NIR transitions for **PBI-Ph**.

Transitions	% character	λ_{cal} [nm]	Oscillator strength f
188 → 189	100	570.60	0.3555
186 → 190	2.37	386.66	0.0718
187 → 189	94.8		
188 → 193	2.82		
177 → 189	5.17	377.15	0.2671
186 → 189	84.4		
187 → 190	3.47		
188 → 192	6.99		
178 → 189	4.57	344.60	0.0086
179 → 189	69.0		
181 → 189	6.37		
188 → 191	20.0		
176 → 189	2.93	311.14	0.0062
179 → 189	14.6		
187 → 189	3.51		
188 → 191	73.8		
188 → 193	5.22		
175 → 189	17.0	306.00	0.0030
176 → 190	8.68		
177 → 189	9.72		
180 → 189	7.49		
183 → 189	29.4		
185 → 189	20.0		
186 → 191	2.51		
188 → 190	5.20		
172 → 191	2.34	307.70	0.0023
175 → 190	16.6		
176 → 189	68.7		
176 → 195	5.10		
177 → 190	3.96		
188 → 191	3.26		
175 → 189	28.9	303.94	0.0079
176 → 190	11.9		
177 → 189	16.6		
180 → 189	4.13		
183 → 189	28.4		
185 → 189	6.71		
188 → 190	3.30		

Table S15 Calculated UV/Vis/NIR transitions for **PBI-Ph⁻**.

Transitions	% character	λ_{cal} [nm]	Oscillator strength f
189A → 190A	26.8	821.94	0.0108
185B → 190B	1.52		
188B → 189B	71.7		
185A → 191A	1.66	679.33	0.4376
189A → 190A	72.5		
189A → 193A	1.31		
185B → 190B	1.55		
188B → 189B	23.0		
188A → 200A	1.28	626.34	0.0888
189A → 191A	97.6		
186B → 189B	1.12		
188A → 191A	7.39	503.73	0.0035
188A → 194A	2.47		
189A → 192A	70.1		
189A → 202A	8.49		
184B → 189B	2.05		
187B → 189B	3.79		
188B → 191B	5.68		
188A → 192A	6.02	456.13	0.0041
188A → 202A	1.17		
189A → 194A	78.0		
189A → 199A	6.10		
189A → 201A	7.53		
188B → 192B	1.18		
188A → 191A	13.8	426.04	0.0184
189A → 192A	17.7		
189A → 200A	6.95		
170B → 189B	1.62		
184B → 189B	10.4		
187B → 189B	26.0		
188B → 191B	23.6		
183A → 193A	1.29	399.00	0.0318
186A → 192A	5.49		
187A → 191A	1.23		
188A → 195A	4.49		
189A → 193A	83.6		
189A → 204A	1.59		
186B → 192B	2.31		
188A → 191A	1.62	382.54	0.0111
180B → 191B	1.17		
184B → 189B	35.9		
186B → 190B	6.89		
187B → 189B	49.7		
188B → 191B	4.74		

Table S16 Calculated UV/Vis/NIR transitions for **PBI-Ph²⁻**.

Transitions	% character	λ_{cal} [nm]	Oscillator strength f
189 → 190 189 → 193	92.9 7.11	575.80	0.5119
189 → 191 189 → 199	96.6 3.45	548.14	0.2973
189 → 192 189 → 200 189 → 202	93.3 3.18 3.52	520.90	0.0359
188 → 192 189 → 194 189 → 199 189 → 201	2.52 50.9 31.5 15.0	450.41	0.0440
189 → 190 189 → 193	7.55 92.4	433.96	0.1845
189 → 192 189 → 95 189 → 200	2.11 95.4 2.48	387.68	0.0106
189 → 194 189 → 199	48.1 51.9	374.13	0.0375

Table S17 Calculated UV/Vis/NIR transitions for **PBI-OPh**.

Transitions	% character	λ_{cal} [nm]	Oscillator strength f
204 → 205	100	477.05	0.6518
194 → 205	2.48	359.77	0.2252
197 → 205	3.52		
202 → 205	10.4		
203 → 205	83.6		
197 → 205	6.19	348.76	0.1206
201 → 205	12.0		
202 → 205	72.6		
203 → 205	9.12		
197 → 205	5.08	303.96	0.0225
201 → 205	62.7		
202 → 205	22.6		
203 → 207	4.36		
204 → 207	5.25		
189 → 205	5.99	298.51	0.0031
204 → 206	94.0		
187 → 205	3.95	292.17	0.0130
188 → 205	4.29		
190 → 205	11.8		
197 → 205	23.1		
198 → 205	2.68		
199 → 205	7.84		
200 → 205	10.2		
203 → 205	9.09		
204 → 207	22.9		
204 → 208	4.16		
188 → 205	5.82	290.90	0.0156
190 → 205	5.06		
194 → 205	9.93		
197 → 205	4.03		
199 → 205	7.11		
200 → 205	25.6		
201 → 205	11.0		
204 → 207	31.5		

Table S18 Calculated UV/Vis/NIR transitions for **PBI-OPh⁻**.

Transitions	% character	λ_{cal} [nm]	Oscillator strength f
205A → 206A	73.3	767.46	0.0624
204B → 205B	26.7		
204A → 217A	1.17	634.20	0.0644
205A → 207A	98.8		
198A → 207A	1.47	570.46	0.6470
205A → 206A	25.6		
198B → 206B	1.99		
204B → 205B	70.9		
204A → 218A	2.11	424.98	0.0117
205A → 208A	22.4		
205A → 210A	2.70		
205A → 211A	3.70		
205A → 212A	22.5		
205A → 213A	8.06		
205A → 214A	32.7		
205A → 215A	4.50		
205A → 218A	1.33		
204A → 207A	1.24	356.10	0.1527
196B → 205B	3.21		
197B → 205B	5.12		
202B → 205B	3.42		
202B → 206B	2.46		
203B → 205B	79.4		
203B → 206B	5.11		
204A → 207A	2.82	349.43	0.0285
195B → 205B	1.44		
196B → 205B	6.79		
201B → 205B	6.44		
202B → 205B	72.6		
202B → 206B	5.76		
203B → 205B	1.73		
203B → 206B	2.39		
204A → 207A	6.83	328.69	0.0108
205A → 210A	5.16		
205A → 212A	4.90		
205A → 214A	1.64		
205A → 217A	11.1		
205A → 218A	17.5		
196B → 205B	20.4		
204B → 207B	32.4		

Table S19 Calculated UV/Vis/NIR transitions for **PBI-OPh²⁻**.

Transitions	% character	λ_{cal} [nm]	Oscillator strength f
205 → 206	4.54	555.80	0.2046
205 → 207	70.3		
205 → 208	2.66		
205 → 209	18.0		
205 → 211	4.50		
205 → 206	97.2	550.25	0.7577
205 → 207	2.82		
205 → 207	6.39	430.38	0.0355
205 → 208	26.6		
205 → 209	22.4		
205 → 210	2.30		
205 → 211	3.78		
205 → 212	5.88		
205 → 216	30.3		
205 → 221	2.32		
205 → 208	45.1	429.54	0.0054
205 → 209	10.4		
205 → 210	17.0		
205 → 211	3.23		
205 → 212	2.60		
205 → 213	8.10		
205 → 217	4.71		
205 → 220	4.83		
205 → 222	3.98		
205 → 207	4.40	412.89	0.0018
205 → 208	12.5		
205 → 209	40.8		
205 → 210	31.9		
205 → 211	5.27		
205 → 213	5.03		
205 → 207	14.0	396.20	0.0321
205 → 208	9.85		
205 → 209	11.5		
205 → 210	15.8		
205 → 212	20.5		
205 → 216	28.4		
205 → 207	3.88	392.47	0.0241
205 → 210	17.9		
205 → 211	73.9		
205 → 212	4.27		
205 → 208	9.04	380.94	0.0126
205 → 210	17.0		
205 → 211	5.89		
205 → 212	13.9		
205 → 213	21.5		
205 → 216	20.4		
205 → 217	3.10		
205 → 219	3.32		
205 → 220	5.89		
205 → 211	4.97	363.43	0.0446
205 → 212	56.2		
205 → 213	30.7		
205 → 216	8.15		
205 → 213	3.38	350.44	0.0162
205 → 214	93.9		
205 → 216	2.67		

Table S20 Experimental and calculated transition dipole moments (μ_{eg}) of the PBIs in Debye.

	$\mu_{\text{eg}} \text{ (Experimental) [D]}$ ^[a]			$\mu_{\text{eg}} \text{ (Calculated) [D]}$ ^[b]		
	PBI	PBI ⁻	PBI ²⁻	PBI	PBI ⁻	PBI ²⁻
PBI-CICN	- ^[c]	- ^[c]	- ^[c]	6.7	3.6	9.2
PBI-Cl	8.7	3.8	12.6	7.6	1.7	9.1
PBI-H	8.8	3.4	3.5	8.8	2.2	3.4
PBI-Ph	6.4	3.1	10.0	6.6	8.0	8.0
PBI-OPh	8.7	3.5	12.4	8.1	3.2	9.4

[a] Obtained by integration of the respective S₀-S₁ or D₀-D₁ transition (see Table S21). [b] Taken from the TD-DFT calculations of the absorption spectra performed by the Multiwfn program.^[85] [c] Not determined due to possible significant overestimation as multiple transitions are present in the respective absorption bands.

The transition dipole moment (μ_{eg}) has been calculated from the integral of the lowest energy absorption band according to equation S1

$$|\mu_{\text{eg}}|^2 = \frac{3hc\varepsilon_0 \ln 10}{2\pi^2 N_A} \cdot \int_{\tilde{\nu}_1}^{\tilde{\nu}_2} \frac{\varepsilon(\tilde{\nu})}{\tilde{\nu}} d\tilde{\nu}, \quad (\text{S1})$$

with the molar extinction coefficient $\varepsilon(\tilde{\nu})$, speed of light $c = 2.9979 \cdot 10^{10} \text{ cm s}^{-1}$, Planck's constant $h = 6.6262 \cdot 10^{-34} \text{ Js}$, permittivity $\varepsilon_0 = 8.8542 \cdot 10^{-12} \text{ F m}^{-1}$ and Avogadro's number $N_A = 6.0221 \cdot 10^{23} \text{ mol}^{-1}$.

Table S21 Integration areas for the determination of the transition dipole moments (μ_{eg}) according to equation S1 of the PBIs from the experimental absorption spectra (Table S20).

	PBI	PBI ⁻	PBI ²⁻
PBI-Cl	440-580 nm	980-1125 nm	530-760 nm
PBI-H	400-600 nm	900-1025 nm	630-700 nm
PBI-Ph	510-715 nm	1010-1285 nm	525-735 nm
PBI-OPh	480-625 nm	1030-1165 nm	515-790 nm

6. Supporting References

- [S1] B. Pagoaga, L. Giraudet and N. Hoffmann, *Eur. J. Org. Chem.*, 2014, 5178-5195.
- [S2] J. Heitmüller, K. Eckstein, R. Renner, M. Stolte, T. Hertel, F. Würthner and T. Brixner, *Spectrochim Acta, Part A*, 2021, **253**, 119567.
- [S3] G. Seybold and G. Wagenblast, *Dyes Pigm.*, 1989, **11**, 4, 303-317.
- [S4] Gaussian 16, Revision C.01, M. J. Frisch, G. W. Trucks, H. B. Schlegel, G. E. Scuseria, M. A. Robb, J. R. Cheeseman, G. Scalmani, V. Barone, G. A. Petersson, H. Nakatsuji, X. Li, M. Caricato, A. V. Marenich, J. Bloino, B. G. Janesko, R. Gomperts, B. Mennucci, H. P. Hratchian, J. V. Ortiz, A. F. Izmaylov, J. L. Sonnenberg, D. Williams-Young, F. Ding, F. Lipparini, F. Egidi, J. Goings, B. Peng, A. Petrone, T. Henderson, D. Ranasinghe, V. G. Zakrzewski, J. Gao, N. Rega, G. Zheng, W. Liang, M. Hada, M. Ehara, K. Toyota, R. Fukuda, J. Hasegawa, M. Ishida, T. Nakajima, Y. Honda, O. Kitao, H. Nakai, T. Vreven, K. Throssell, J. A. Montgomery, Jr., J. E. Peralta, F. Ogliaro, M. J. Bearpark, J. J. Heyd, E. N. Brothers, K. N. Kudin, V. N. Staroverov, T. A. Keith, R. Kobayashi, J. Normand, K. Raghavachari, A. P. Rendell, J. C. Burant, S. S. Iyengar, J. Tomasi, M. Cossi, J. M. Millam, M. Klene, C. Adamo, R. Cammi, J. W. Ochterski, R. L. Martin, K. Morokuma, O. Farkas, J. B. Foresman, and D. J. Fox, Gaussian, Inc., Wallingford CT, 2016.
- [S5] T. Lu and F. Chen, *J. Comput. Chem.*, 2012, **33**, 580-592.
- [S6] W. Yue, W. Jiang, M. Bockmann, N. L. Doltsinis and Z. H. Wang, *Chem. Eur. J.*, 2014, **20**, 5209-5213.
- [S7] S. Seifert, D. Schmidt and F. Würthner, *Chem. Sci.*, 2015, **6**, 1663-1667.
- [S8] J. Sworakowski, J. Lipiński and K. Janus, *Org. Electron.*, 2016, **33**, 300-310.
- [S9] S. J. Borg and S. P. Best, *J. Electroanal. Chem.*, 2002, **535**, 57-64.